

# A BOUNDARY ELEMENT FORMULATION BASED ON THE THREE-DIMENSIONAL ELASTOSTATIC FUNDAMENTAL SOLUTION FOR THE INFINITE LAYER: PART II—THREE-DIMENSIONAL EXAMPLES

L. LU\*

*Division of Engineering and Applied Sciences, California Institute of Technology, 105-50, Pasadena, CA 91125, U.S.A.*

F. G. BENITEZ†

*Department of Mechanical Engineering, University of Sevilla, Avda, Reina Mercedes, Sevilla-41012, Spain*

AND

A. J. ROSAKIS‡

*Division of Engineering and Applied Sciences, California Institute of Technology, 105-50, Pasadena, CA 91125, U.S.A.*

## SUMMARY

This work applies the specialization of the integral identities used in the boundary element method to the numerical solution of three-dimensional elasticity problems involving geometries containing two parallel planar surfaces (see Part I this issue). Two three-dimensional problems are numerically analysed by using the above procedure. These are the problems of pressurized circular and elliptical holes in infinite plates of uniform thickness. For the circular hole problem, the accuracy of our scheme is established by direct comparison of our results with the available analytical solution. For the ellipse problem, with an aspect ratio of 4:1, the boundary element results are compared with those of a finite element calculation.

## 1. INTRODUCTION

In a wide range of engineering applications, two-dimensional idealizations of three-dimensional problems have been considered acceptable mainly for two reasons: (i) the modelling is, in many cases, conservative compared to its three-dimensional counterparts, and (ii) three-dimensional geometries are more complex from a computational point of view. However, in three-dimensional problems exhibiting high gradients of stress and strain fields, two-dimensional idealizations are often inadequate.

Finite element solutions applied to the modelling of the above-mentioned problems have been extensively reviewed in the literature; see, for example, References 1–3.

One of the key issues in the application of finite elements to problems exhibiting high gradients of stress and strain is the choice of the number and size of the elements used in the region where

---

\* Graduate Student

† Professor

‡ Associate Professor

these high gradients appear. Thus, if small elements are used in the modelling of this region, the finite element approach, although extremely versatile, may require models with a very high number of degree of freedom. Another approach based on the use of special elements suitable for approximating high gradients of functions has been extensively used in order to reduce the number of elements in the models. Both approaches are now widely known and are referenced in most finite element books.

The boundary element method (BEM) developed in a similar way. The publications by Cruse<sup>4-12</sup> on the use of this technique for high stress concentration problems and on the effect of increasing the level of discretization are well known. Moreover, the studies of Weaver,<sup>13</sup> Blandford *et al.*<sup>14</sup> and Luchi and Poggialini<sup>15</sup> on the use of special elements followed equivalent developments in finite elements.

At this stage, the great advantage provided by the boundary element technique in reducing the dimensionality of the problem by one makes it very attractive for the analysis of three-dimensional geometries. Although this advantage is greatly reduced by the fact that the technique is only applicable in potential theory, the possibility of using different fundamental solutions (e.g. Kelvin or Mindlin solutions) broadens the scope. In particular, one recalls the importance of using the solution obtained by Mindlin for a three-dimensional semi-infinite space for analysing problems involving a single infinite planar surface. Along the same lines, other fundamental solutions may be useful in the analysis of other classes of problems. The problem of obtaining specialized Green's functions for the solution of specific problems has received considerable attention since the work done by Kelvin.

In 1985 and 1987, Benitez and Rosakis<sup>16,17</sup> published the three-dimensional elastostatic fundamental solution for a point load in an infinite elastic layer. The basic idea of using this fundamental solution in a boundary element scheme was presented by the same authors in 1988.<sup>18</sup>

In Part I of this investigation we present the complete development of this idea. This includes a detailed derivation of the modified integral identities appropriate for the analysis of three-dimensional problems in geometries involving two parallel planar surfaces. It also contains details of the numerical implementation of the new scheme and the fundamental solution as well as a basic error analysis.

In Part II of this investigation we present the first applications of this approach to the analysis of two three-dimensional elastostatic problems. These problems involve pressurized circular and elliptical holes in plates of uniform finite thickness. The two examples are used to establish the accuracy of the proposed scheme. A more detailed study can be found in Lu.<sup>19</sup>

## 2. CIRCULAR HOLE SUBJECTED TO INTERNAL PRESSURE

The problem involves a circular hole in an infinite plate of uniform thickness subjected to uniform internal pressure applied on the surface of the hole. Furthermore, the upper and the lower surfaces of the plate are traction free. Although this testing problem is a fully three-dimensional one, its solution happens to coincide with both the plane-strain and plane-stress solutions for the corresponding two-dimensional problems with the same in-plane geometry and loading. By taking advantage of this fact, we use this known solution as a benchmark case for comparison with our three-dimensional BEM computations. Further comparison is provided by a (FEM) calculation. Once agreement between theory and numerics is demonstrated in this simple case, the solution of a more complex three-dimensional problem will be attempted.

2.1. Analytical solution

Consider the problem of a pressurized circular hole (surface  $L_1$ ) of radius  $a$  in an infinite plate of uniform thickness  $h$ . The upper and lower surfaces ( $\Pi_1$  and  $\Pi_2$ ) of the plate are traction free. Figure 1 shows the problem schematically.

By denoting the tractions as  $\mathbf{t}(\mathbf{x}, \mathbf{n})$ , where  $\mathbf{x} = r\mathbf{e}_r + \theta\mathbf{e}_\theta + x_3\mathbf{e}_3$  and  $\mathbf{n} = n_r\mathbf{e}_r + n_\theta\mathbf{e}_\theta + n_3\mathbf{e}_3$ , the boundary conditions become

$$\begin{aligned} \mathbf{t}(\mathbf{x}, \mathbf{e}_3) &= \mathbf{0}, \quad \forall \mathbf{x} \in \Pi_1 \\ \mathbf{t}(\mathbf{x}, -\mathbf{e}_3) &= \mathbf{0}, \quad \forall \mathbf{x} \in \Pi_2 \\ \mathbf{t}(\mathbf{x}, -\mathbf{e}_r) &= -p\mathbf{e}_r, \quad \forall \mathbf{x} \in L, p > 0 \end{aligned} \tag{1}$$

where  $p$  is the magnitude of the applied pressure and vectors  $\mathbf{e}_r, \mathbf{e}_\theta, \mathbf{e}_3$  are the unit vectors of the cylindrical co-ordinate system.

The in-plane stress field corresponding to the plane-strain and plane-stress approximation of this three-dimensional problem are given in Reference 20 as follows:

$$\left. \begin{aligned} \sigma_{\theta\theta}(r, \theta) &= -\sigma_{rr}(r, \theta) = \frac{a^2}{r^2} p, \\ \sigma_{r\theta}(r, \theta) &= 0, \end{aligned} \right\} \quad \forall r \geq a \quad \forall 0 \leq \theta \leq 2\pi \tag{2}$$

From the former expressions and the constitutive law,

$$\begin{aligned} \varepsilon_{33}(r, \theta) &= \frac{1}{E} [\sigma_{33}(r, \theta) - \nu(\sigma_{rr}(r, \theta) + \sigma_{\theta\theta}(r, \theta))] = \frac{1}{E} \sigma_{33}(r, \theta) \\ \varepsilon_{3r}(r, \theta) &= \frac{1}{\mu} \sigma_{3r}(r, \theta) \\ \varepsilon_{3\theta}(r, \theta) &= \frac{1}{\mu} \sigma_{3\theta}(r, \theta) \end{aligned} \tag{3}$$

The above equations imply that, for both the plane-strain and plane-stress idealizations,  $\varepsilon_{3i}(r, \theta)$  and  $\sigma_{3i}(r, \theta)$  are zero simultaneously.

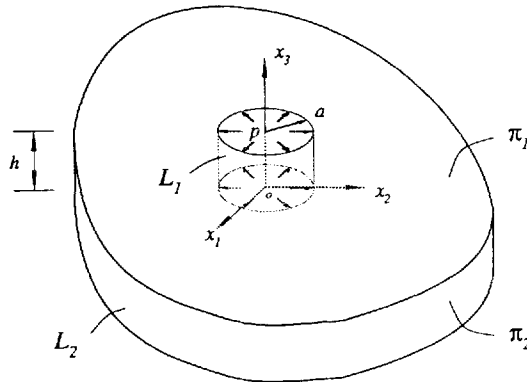


Figure 1. Pressurized circular hole in an infinite plate

In addition, the displacement fields for both cases are identical and given by

$$\begin{aligned}u_r(r, \theta) &= \frac{1}{2\mu} \frac{a^2}{r} p \\u_\theta(r, \theta) &= 0 \\u_3(r, \theta) &= 0\end{aligned}\tag{4}$$

where  $\mu$  and  $E$  denote the shear and Young moduli, respectively, for the linear elastic solid.

The fact that the plane-strain and plane-stress solutions of this three-dimensional problem coincide (identical stresses, displacements and strains) suggests the possibility that these two-dimensional solutions may also be the solution of the fully three-dimensional problem. Indeed, if the above solution, expressions (2)–(4), are substituted in the three-dimensional governing equations for linear elastostatics, these equations are satisfied identically. Furthermore, the uniqueness theorem of linear elastostatics guarantees that (2)–(4) furnish the only solution of the three-dimensional problem satisfying the given boundary conditions (1). In addition, the boundary conditions given by expression (1) on the surfaces of the plate  $\Pi_2$  and  $L_1$  are trivially satisfied.

## 2.2. Modelling of the circular hole surface and boundary element mesh

In order to compute tractions and displacements at the boundary, the boundary integral equation given by expression (45) in Part I has to be evaluated.

As long as the upper and lower surfaces of the plate are traction-free, only the lateral surfaces need to be discretized. The lateral surface is the surface of the hole  $L_1$ . This is the key difference between the modified boundary element scheme and the conventional one, which employs the Kelvin solution as the fundamental solution.

Two mesh schemes are employed for the modified boundary element scheme, in which 160 and 640 elements are used.

Call the dimension of an element in the  $x_3$  direction the element thickness and the corresponding dimension in the circular direction the width. All the elements used have the same width, and the elements in a layer have the same thickness.

In general, the circular hole is modelled by flat rectangular elements of the same width. The thickness direction of the hole is modelled by five and ten layers of elements for the 160-element and 640-element meshes, respectively.

When constant elements are used, the node of each element is located at its centroid. The displacement and traction are computed only at the element centroid.

In the numerical computation of the fundamental solution for the three-dimensional infinite layer, as stated in paragraph 5.2 of Part I, the pre-set number  $P$  is chosen to be 10 or 20. For justification of this choice, see the error analysis section of Part I of this investigation.

Two groups (A and B) of internal points are placed in the interior of the plate. The 51 internal points in Group A are selected to examine the displacement variation along the radius direction; the 15 internal points in Group B are required to observe the displacement variation through the thickness.

The points in Group A are placed in three radial arrays at different depths inside the plate. All the arrays contain the same number of points (17 points each), and the points in the three arrays have the same radial positions. The first and second array of points are placed in planes 1 and 25 per cent of the thickness from the top surface of the plate, respectively, and the third array is placed in the mid-plane of the plate. Since the displacement field is expected to exhibit a higher

gradient with respect to  $r$  near the surface of the hole, the points in each array are placed closer to each other when they are near the circular hole surface, and further apart when they are away from the hole surface. The positions of the points in the  $r$  direction are:

$$\begin{aligned} r = & a + 0.01h, \quad a + 0.05h, \quad a + 0.10h, \quad a + 0.20h \\ & a + 0.30h, \quad a + 0.40h, \quad a + 0.50h, \quad a + 0.60h \\ & a + 0.70h, \quad a + 0.80h, \quad a + 0.90h, \quad a + 1.00h \\ & a + 1.10h, \quad a + 1.20h, \quad a + 1.30h, \quad a + 1.40h \\ & a + 1.50h \end{aligned}$$

where  $h$  stands for the plate thickness, and  $a$  stands for the radius of the hole, chosen to be  $a = 1.00h$ .

The points in Group B are positioned along a line through the thickness of the plate. On this line, the displacement is evaluated at 15 points. The position of the line is  $r = 1.05h$ . The positions of the points on the line are

$$\begin{aligned} x_3 = & 0.00h, \quad 0.01h, \quad 0.05h, \quad 0.10h \\ & 0.20h, \quad 0.30h, \quad 0.40h, \quad 0.50h \\ & 0.60h, \quad 0.70h, \quad 0.80h, \quad 0.90h \\ & 0.95h, \quad 0.99h, \quad 1.00h \end{aligned}$$

The cross section of the circular hole in the first and second mesh arrangement is modelled by 32 and 64 equally sized elements, respectively. In the thickness direction, the hole is modelled by five and ten layers of elements, the layers having a regular thickness of  $0.2h$  and  $0.1h$ , respectively.

The positions of the Group A points in the  $x_3$  direction are  $x_3 = 0.99h, 0.75h$  and  $0.50h$ .

The arrangements of the elements and the internal points are sketched in Figure 2 for the 160-element mesh.

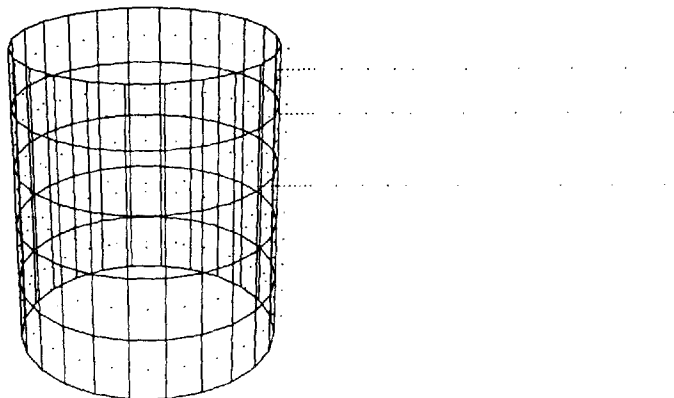


Figure 2. 160-element mesh for the hole surface. The elements are distributed in five layers

### 2.3. Results and error analysis

In this section the numerical results obtained from the boundary element method are plotted against the analytical solution. In all the calculations, Young's modulus  $E$  and Poisson's ratio  $\nu$  were chosen to be 1 and 0.3, respectively.

In Figures 3–8, the normalized displacement components  $u_r$  and  $u_3$  versus the normalized radius  $r$  for the points in Group A, and the same displacement components versus the normalized

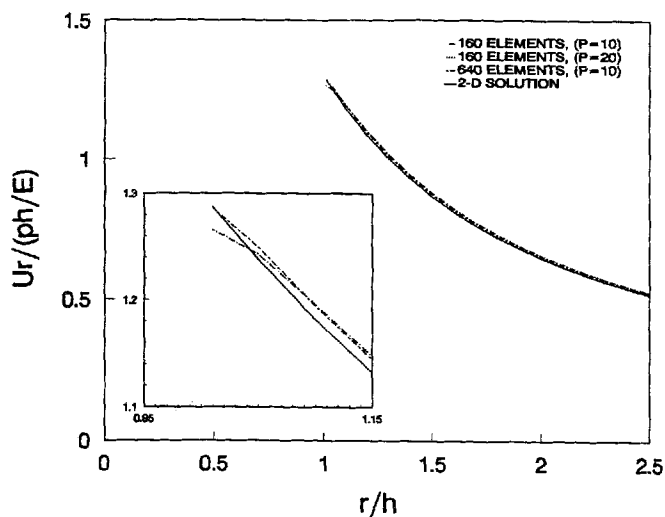


Figure 3. Normalized displacement  $u_r$  versus normalized distance  $r$ . Results obtained at a depth of 1 per cent from the top surface,  $x_3 = 0.99h$

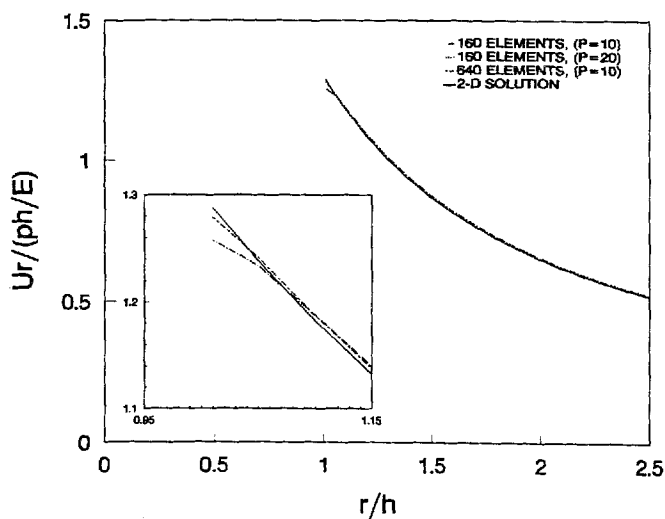


Figure 4. Normalized displacement  $u_r$  versus normalized distance  $r$ . Results obtained at a depth of 25 per cent from the top surface,  $x_3 = 0.75h$

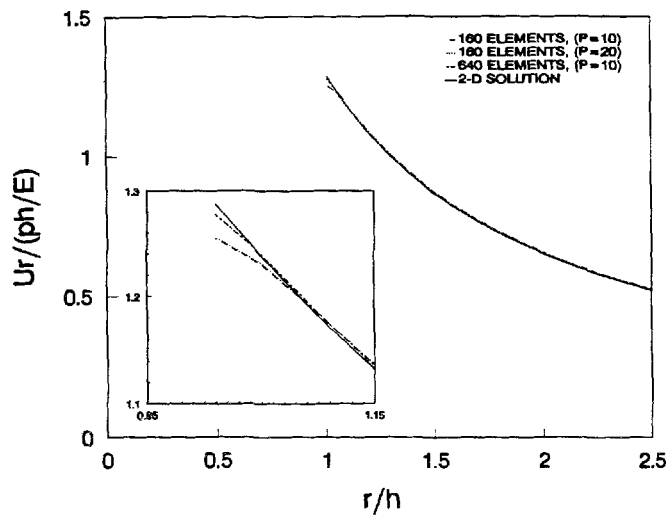


Figure 5. Normalized displacement  $u_r$  versus normalized distance  $r$ . Results obtained at the median plane of the plate,  $x_3 = 0.5h$

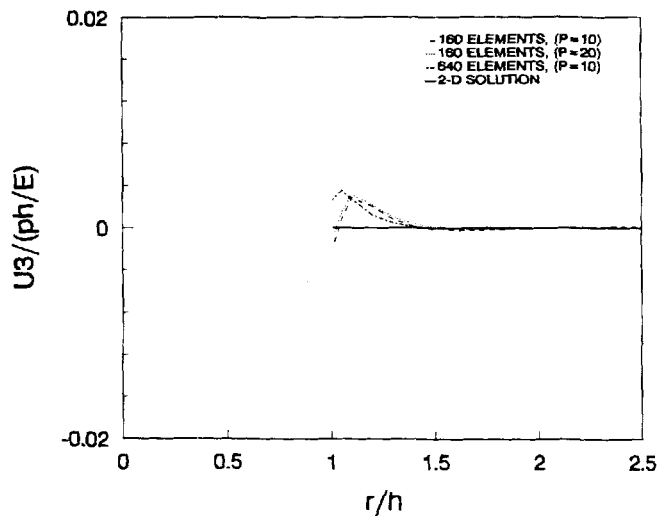


Figure 6. Normalized displacement  $u_3$  versus normalized distance  $r$ . Results obtained at a depth of 1 per cent from the top surface,  $x_3 = 0.99h$

depths of the points in Group B are shown. The surface of the hole is at  $r/h = 1$  and  $0 \leq x_3/h \leq 1.0$ .

Figures 3–5 show the variations of the displacement component  $u_r$  as a function of  $r/h$ . These points belong to Group A. Each figure is associated with a different cross section of the plate. It is shown that the BEM and analytical solutions are virtually indistinguishable. The results show that for the 160-element mesh arrangement the displacements obtained when P is set to 10 and 20

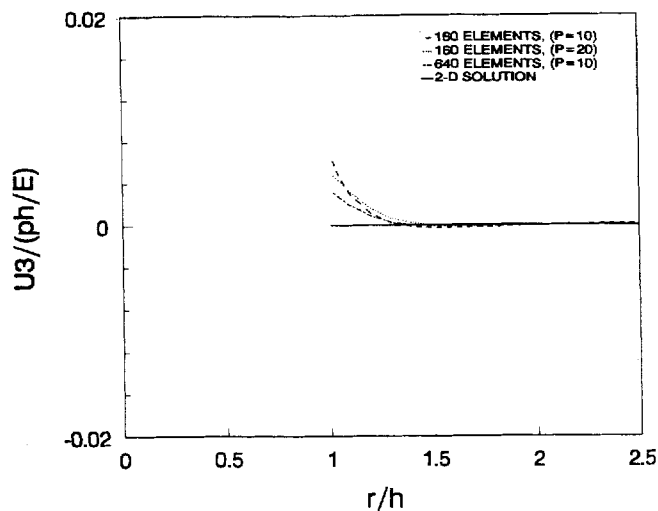


Figure 7. Normalized displacement  $u_3$  versus normalized distance  $r$ . Results obtained at a depth of 25 per cent from the top surface,  $x_3 = 0.75h$

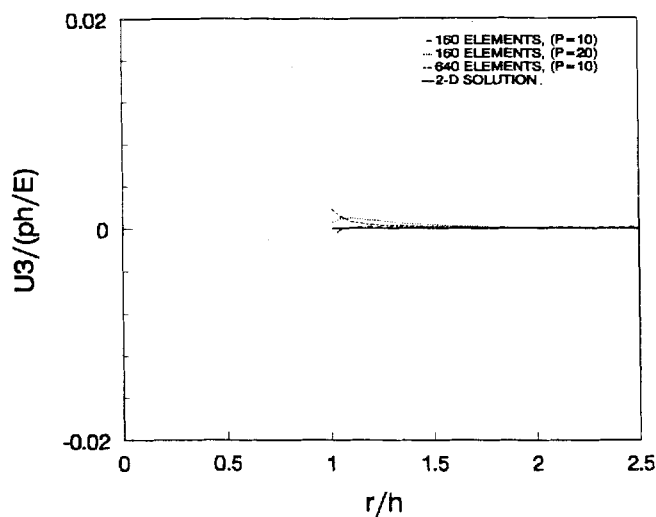


Figure 8. Normalized displacement  $u_3$  versus normalized distance  $r$ . Results obtained at the median plane of the plate,  $x_3 = 0.5h$

are virtually on top of each other. At points which are close to the surface of the hole, the solution shows deviation between 160- and 640-element meshes, although this deviation is of the order of less than 3 per cent.

Figures 6–8 show the variations of the out-of-plane displacement component as a function of normalized distances from the centre of the hole. In this particular case, the three-dimensional boundary element solution agrees well with the analytical predictions up to a distance of

approximately twice the maximum dimension of the nearest element on the hole surface. This error, less than 1 per cent, is due to the discretization coarseness and decreases with decreasing element size, as can be inferred from the improvement in the results obtained for the 640-element mesh compared to the 160-element mesh.

Figure 9 shows the variations of the displacement component  $u_r$  through the plate thickness. Figure 10 shows the variations of the displacement component  $u_3$  through the plate thickness.

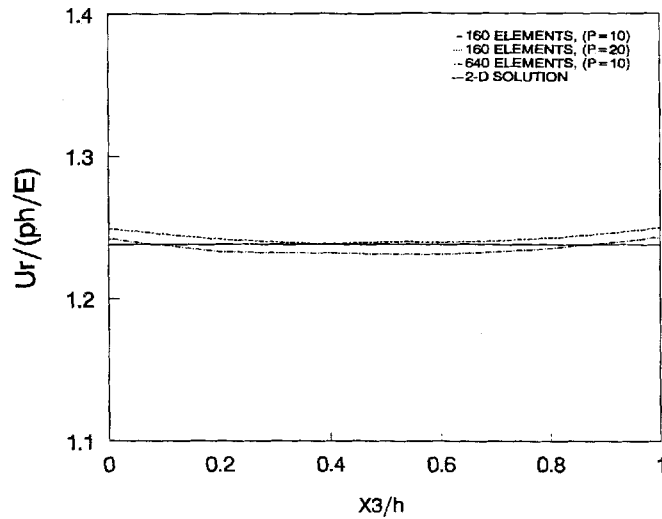


Figure 9. Normalized displacement  $u_r$  versus normalized depth  $x_3$ . Results obtained at a normalized distance of  $0.05h$  from the hole surface

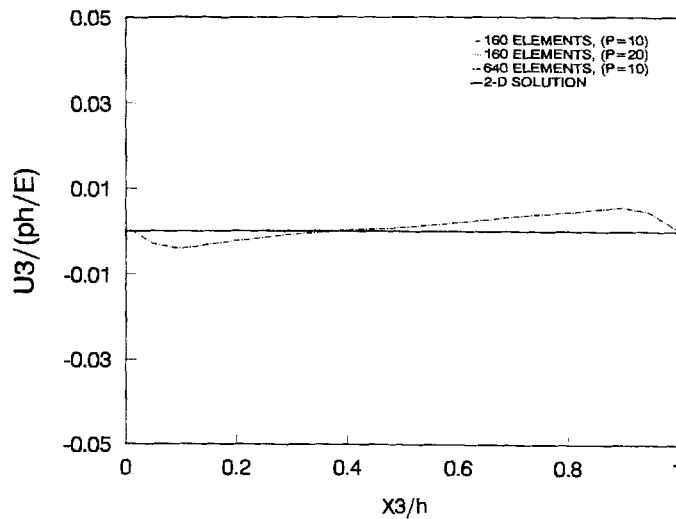


Figure 10. Normalized displacement  $u_3$  versus normalized depth  $x_3$ . Results obtained at a normalized distance of  $0.05h$  from the hole surface

Again, very good agreement between the numerical solution and the analytical prediction is shown.

The accuracy of the final result depends on the following two aspects. First, the surface of the subject has to be modelled precisely, and second, the numerical integration of the above integrals over each patch (element) of the modelled surface must be computed accurately.

Both these aspects leave room for error. One possibility is discretization error, which in this case includes two major parts: the geometry mismatch caused by using flat elements, and the assumption that the displacement and traction are constant over an element. Another possibility is the error resulting from the evaluation of the stress and the displacement components of the fundamental solution for the three-dimensional infinite layer problem. As shown from the above results, a choice of  $P = 10$  seems to be adequate. Preliminary calculations for  $P = 10$  produce results that exhibit a maximum deviation from the analytical solution of 1 per cent.

### 3. ELLIPTICAL HOLE SUBJECTED TO INTERNAL PRESSURE

This section considers an elliptical hole in a three-dimensional infinite plate of uniform thickness  $h$  subjected to uniform internal pressure. The ratio of the major to the minor axis is 4. The upper and lower surfaces of the plate are traction free. The geometry and loading of the problem is similar to the one shown in Figure 1. In this problem, the displacement and stress field near the elliptical hole are expected to be three-dimensional in nature. Unlike the equivalent problem of a pressurized circular hole, an analytical solution is not available in three dimensions.

The available plane-strain or plane-stress approximations to this problem will be used for comparison with the numerical BEM and FEM results. The purpose of such a comparison is to identify the regions near the hole where three-dimensional effects are dominant.

#### 3.1. Two-dimensional solutions

Consider the two-dimensional problem of a pressurized elliptical hole in an infinite elastic solid. The major and minor axes of the ellipse are denoted by  $a$  and  $b$ , respectively (see Figure 11). The magnitude of the applied pressure is  $p$ , while  $\mu$  and  $\nu$  denote the shear modulus and Poisson's ratio of the solid, respectively.

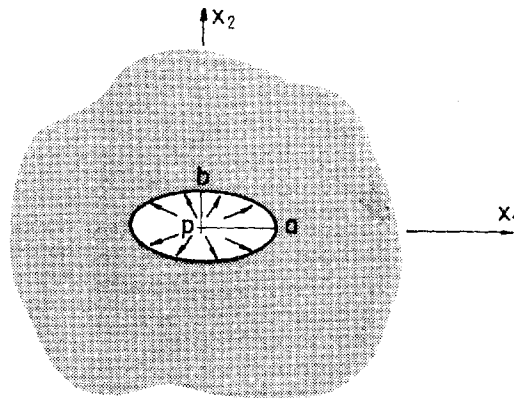


Figure 11. Two-dimensional pressurized elliptical hole on an infinite plate

On the hole boundary, the tractions are given by

$$\mathbf{t} = -p\mathbf{n}, \quad p > 0 \text{ on } \Gamma \quad (5)$$

where  $\mathbf{n}$  is the inward normal to the ellipse.

The solution of this two-dimensional problem can easily be inferred from the problem of a traction-free elliptical hole subjected to remote uniform stress, by superposition; see Reference 20.

For plane-stress the in-plane displacement field is given in elliptical co-ordinates  $(\xi, \eta)$  by

$$\begin{aligned} u_1(\xi, \eta) = & \frac{1}{2\mu(\cos^2 \eta \sinh^2 \xi + \sin^2 \eta \cosh^2 \xi)} \\ & \times \{ -Ac[\sin \eta \sinh \xi(\cos \eta \sin \eta \sinh^2 \xi + \cos \eta \sin \eta \cosh^2 \xi) \\ & + \cos \eta \cosh \xi(\cos^2 \eta \cosh \xi \sinh \xi - \sin^2 \eta \cosh \xi \sinh \xi)] - Bc \cos \eta \sinh \xi \} \\ & + Ac \frac{3-\nu}{2\mu(1-\nu)} \cos \eta \sinh \xi + Ac \frac{\nu-1}{\mu(1+\nu)} \cos \eta \cosh \xi \end{aligned} \quad (6)$$

$$\begin{aligned} u_2(\xi, \eta) = & \frac{1}{2\mu(\cos^2 \eta \sinh^2 \xi + \sin^2 \eta \cosh^2 \xi)} \\ & \times \{ -Ac[\cos \eta \cosh \xi(\cos \eta \sin \eta \sinh^2 \xi + \cos \eta \sin \eta \cosh^2 \xi) \\ & - \sin \eta \sinh \xi(\cos^2 \eta \cosh \xi \sinh \xi - \sin^2 \eta \cosh \xi \sinh \xi)] - Bc \sin \eta \cosh \xi \} \\ & + Ac \frac{3-\nu}{2\mu(1-\nu)} \sin \eta \cosh \xi + Ac \frac{\nu-1}{\mu(1+\nu)} \sin \eta \sinh \xi \end{aligned} \quad (7)$$

where

$$\begin{aligned} A = \frac{p}{2}, \quad B = -\frac{p}{2} \cosh 2\xi_0, \quad \xi_0 = \tanh^{-1} \left( \frac{b}{a} \right) \\ \xi = \ln \frac{\alpha + \beta}{c}, \quad \eta = \begin{cases} \sin^{-1} \left( \frac{x_2}{c \sinh \xi} \right) & \text{for } x_2 \geq 0 \\ \pi - \sin^{-1} \left( \frac{x_2}{c \sinh \xi} \right) & \text{for } x_2 < 0 \end{cases} \end{aligned} \quad (8)$$

$c$  stands for half the distance between the foci of the ellipse, and

$$\begin{aligned} \alpha = \sqrt{\frac{x_1^2 + x_2^2 + c^2 + \sqrt{(x_1^2 + x_2^2 - c^2)^2 + 4x_2^2 c^2}}{2}} \\ \beta = \sqrt{\frac{x_1^2 + x_2^2 - c^2 + \sqrt{(x_1^2 + x_2^2 - c^2)^2 + 4x_2^2 c^2}}{2}} \end{aligned} \quad (9)$$

Under the plane-stress approximation, the out-of-plane displacement  $u_3$  of the original three-dimensional problem (elliptical hole in a plate) is non-zero and given by

$$u_3(x_1, x_2, x_3) = \int_{\frac{h}{2}}^{x_3} \varepsilon_{33}(x_1, x_2) dx_3, \quad 0 \leq x_3 \leq h \quad (10)$$

By using the constitutive law and the fact that  $\sigma_{3i} = 0$  for plane stress, the above becomes

$$\begin{aligned} u_3(x_1, x_2, x_3) &= -\frac{\nu}{2\mu(1+\nu)} \left(x_3 - \frac{h}{2}\right) (\sigma_{11} + \sigma_{22}) \\ &= -\frac{\nu}{2\mu(1+\nu)} \left(x_3 - \frac{h}{2}\right) \left[ \frac{2p \sinh 2\xi}{\cosh 2\xi - \cos 2\eta} - 2p \right] \end{aligned} \quad (11)$$

It should be noted that  $u_3(x_1, x_2, x_3)$  as predicted by plane-stress is linear in  $x_3$ .

In the special case of a circular hole ( $c \rightarrow 0$ ),  $\xi \rightarrow \infty$  and  $\eta \rightarrow 0 \forall x_1, x_2$ . Consequently, equation (11) yields  $u_3 = 0$ , as has been shown in the previous section.

The plane-strain solution for this problem can be trivially obtained from the above expressions by substituting  $\nu$  by  $\nu/(1-\nu)$ . In addition, both  $\varepsilon_{33}$  and  $u_3$  vanish identically.

### 3.2. Modelling of the elliptical hole surface and boundary element mesh

Analogous to the circular hole, expression (45) of Part I has to be evaluated. Since the upper and lower surfaces of the plate are traction free, only the lateral surfaces of the elliptical hole need to be discretized.

The Cartesian co-ordinate system for this problem is located in the lower surface of the plate, the origin of the co-ordinate system is at the centre of the elliptical hole, the  $x_1$  axis is in the direction of the major axis of the ellipse, the  $x_2$  axis is in the direction of the minor axis and the  $x_3$  axis is in the thickness direction.

In this problem the ratio of major to minor axes is 4. Two boundary element meshes, involving 280 and 336 elements, are used to model the elliptical hole. The elements are constant rectangular, and all of them are flat. The displacement and the traction variations over an element are assumed to be constant. The cross section of the elliptical hole is modelled by 40 elements with different widths. In the case including 336 elements, the mesh for modelling the cross section is locally refined. The thickness of the hole is modelled by seven layers of elements. All the elements in an element layer have the same thickness. The thicknesses of the layers are  $0.1h, 0.1h, 0.2h, 0.2h, 0.1h$  and  $0.1h$  from the bottom to the top of the plate. The pre-set number  $P$  is chosen to be 10 for both mesh schemes.

Four groups (A, B, C and D) of internal points are used to examine the displacement field inside the plate.

Group A contains 45 internal points, and these are equally divided and placed in three arrays at different depths along the extension of the major axis of the elliptical hole. The first array contains 15 points and it is located at a distance  $x_3 = 0.95h$  from the lower surface, the second array contains the same number of points and its depth is  $0.75h$ , and the third array of points is located in the mid-plane of the plate. The positions of the points in any array in the  $x_1$  direction are:

$$\begin{aligned} x_1 &= a + 0.01h, \quad a + 0.03h, \quad a + 0.05h, \quad a + 0.07h \\ & \quad a + 0.09h, \quad a + 0.13h, \quad a + 0.23h, \quad a + 0.33h, \\ & \quad a + 0.43h, \quad a + 0.50h, \quad a + 0.70h, \quad a + 0.90h \\ & \quad a + 1.10h, \quad a + 1.30h, \quad a + 1.50h \end{aligned}$$

Group B has 33 internal points, and these points are placed in three lines along the thickness direction. The displacements are evaluated at 11 points through the thickness. The lines are positioned at  $x_2 = 0$  and  $x_1 = 0.51h, 0.73h$  and  $1.6h$ . The points are equally spaced in each line.

The first and the last points at both ends of the lines positioned at  $x_2 = 0$  and  $x_1 = 0.51h$  are located at  $x_3 = 0.03h$  and  $0.97h$ , respectively, and at  $x_3 = 0$  and  $x_3 = 1.0h$  for the other two lines.

Groups C and D contain 48 and 22 internal points, respectively. In contrast to the Group A and B points, these points are placed along the extension of the minor axis of the elliptical hole.

Figure 12 shows the model for the 280-element mesh elliptical hole and the arrangement of the internal points.

### 3.3. Finite element analysis

The three-dimensional finite element analysis code FEAP has been adopted in the present study. FEAP was originally developed by R. J. Taylor<sup>24</sup> of U. C. Berkeley and later revised at Brown University. The code was made available through the courtesy of Dr. Ravichandran.

The modelling effort of a three-dimensional problem of a pressurized elliptical hole in an infinite plate can be greatly reduced by taking advantage of the symmetry. In the implementation of the FEAP, one-eighth of the plate is modelled as depicted in Figure 13. The model is bounded by six surfaces: two orthogonal surfaces through the thickness, the top free surface and the midplane of the plate, a quarter of the elliptical surface enclosed between the two orthogonal surfaces and a remote surface.

When the radius of this remote surface is large compared to the radius of the elliptical hole, it can be assumed that stresses and displacements on it are negligible.

Therefore, in the model of the finite element analysis, the three-dimensional plate is truncated by a remote concentric circular surface at the radius of 20 times the thickness of the plate, and traction-free boundary conditions are applied on this remote surface. By analysing the two-dimensional plane-stress solution of the pressurized elliptical hole problem when the remote surface is chosen to be at a radius of about 20 times the thickness, the stress and the displacement at the remote surface are of the order of  $10^{-4}$  and  $10^{-2}$ . It is then assumed that the traction-free boundary conditions can be applied on the remote surface. The finite element mesh is shown in Figures 14 and 15. The mesh is composed 1045 elements with 1440 nodes and 4320 degrees of freedom. All the elements are placed evenly in five element layers. The thickness of the layers from the midplane to the top of the plate are  $0.1h$ ,  $0.15h$ ,  $0.15h$ ,  $0.05h$  and  $0.05h$ .

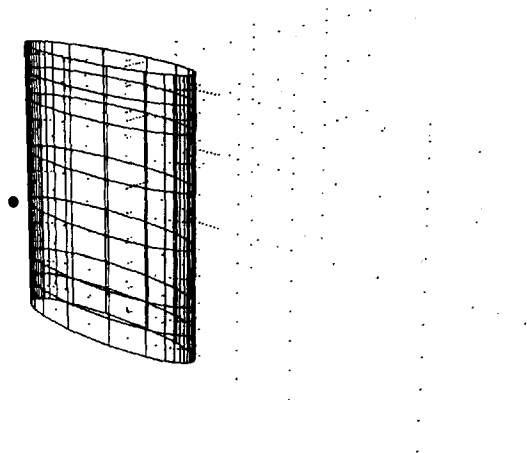


Figure 12. Mesh for the elliptical hole with 280 elements. The elements are distributed in seven layers. The aspect ratio is 4

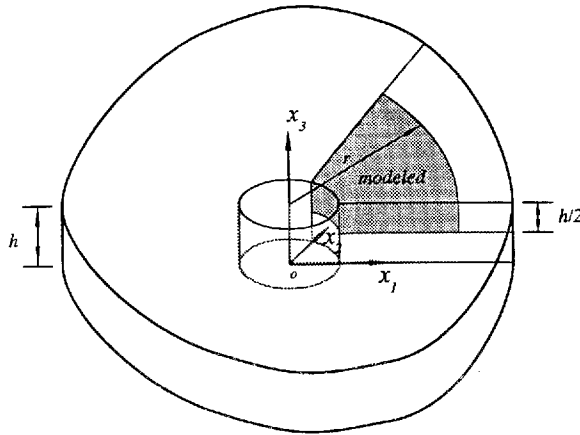


Figure 13. Model for finite element analysis

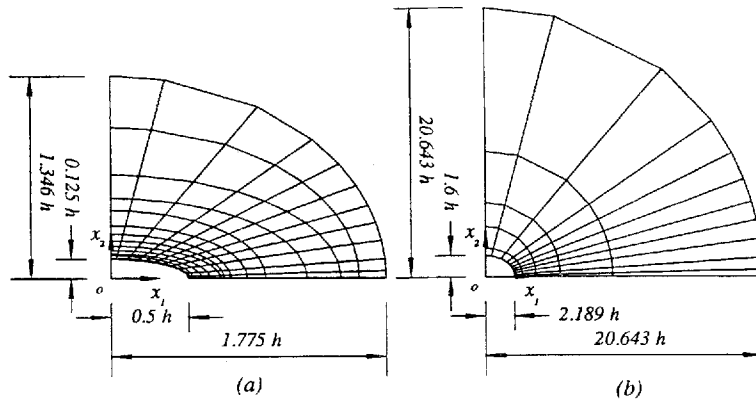


Figure 14. Details of in-plane mesh for finite element analysis, 1045 elements

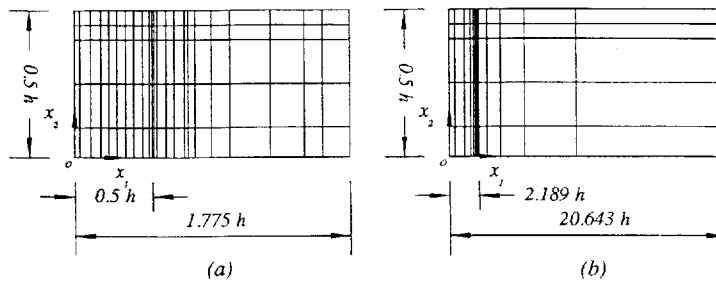


Figure 15. Details of mesh variation through thickness for finite element analysis, 1045 elements

Eight noded tri-linear brick elements are used. The displacement in the interior of an element is evaluated through linearly interpolating the values at the nodes. The stress and strain components are evaluated at the element centroids, which are assumed to be constant within an element. The surfaces of the brick elements along the elliptical hole surface have the same geometries as the elements used for the 280-boundary-element mesh. It is important to point out that the boundary element mesh coincides with the finite element mesh along the surface of the elliptical hole.

The boundary conditions for the finite element model are:

- (i)  $u_2 = 0$  at the nodal points on the  $x_1$ - $x_3$  plane;
- (ii)  $u_1 = 0$  at the nodal points on the  $x_2$ - $x_3$  plane;
- (iii)  $u_3 = 0$  at the nodal points on the  $x_1$ - $x_2$  plane;
- (iv)  $t_1 = t_2 = t_3 = 0$  at the nodal points on the top surface of the plate;
- (v) specified traction boundary conditions on the elliptical hole surface;
- (vi) traction-free boundary conditions of the truncated cylindrical surface.

### 3.4. Results and error analysis

In this section we present representative numerical results obtained by means of the proposed boundary element scheme. The results are compared with those of a finite element calculation modelling the same geometry and loading. In addition, all plots contain analytical predictions obtained by means of the two-dimensional, plane-stress or plane-strain solutions of the same problem [equations (6), (7) and (11)].

The reason for including a comparison of the three-dimensional results with two-dimensional solutions is to identify the regions at the vicinity of the ellipse tip where three-dimensional effects dominate and where the two-dimensional idealizations prove inadequate.

In the following figures the normalized displacement components  $u_1$ ,  $u_2$  and  $u_3$  are plotted versus normalized distances from the ellipse tip, and the thickness variation of the same displacement components is also presented.

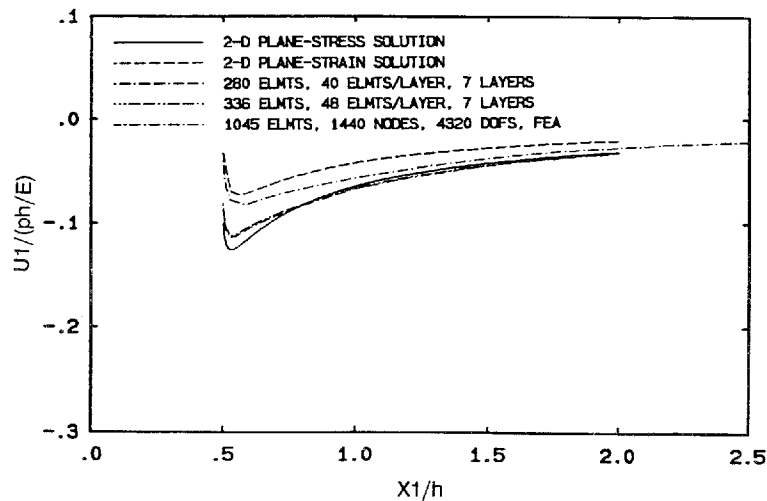


Figure 16. Normalized displacement  $u_1$  versus normalized distance  $x_1$ . Results obtained at a depth of 5 per cent from the top surface,  $x_3 = 0.95h$

The tip of the ellipses is located at  $x_1/h = \pm 0.5$ ,  $x_2 = 0$  and  $0 \leq x_3/h \leq 1.0$ . The elastic constants are chosen to be  $E = 1$  and  $\nu = 0.3$ .

*3.4.1. In-plane displacements.* The two in-plane displacement components do not exhibit strong three-dimensional effects as compared to the out-of-plane displacement. The results of the displacement  $u_1$  computed at different cross sections of the plate (nodal surface  $0.95h$ , three-quarters surface  $0.75h$  and midplane  $0.5h$ ) along the  $x_1$  direction are shown in Figures 16–18; the results of the displacement  $u_2$  evaluated at the same cross sections along the  $x_2$  direction are

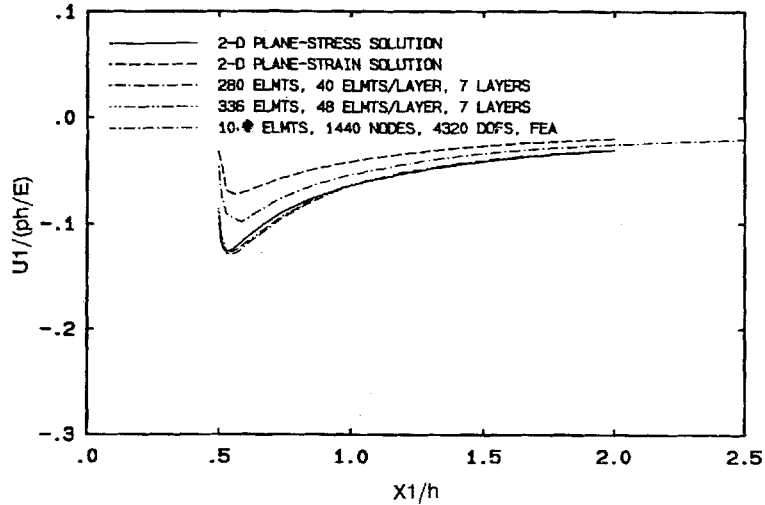


Figure 17. Normalized displacement  $u_1$  versus normalized distance  $x_1$ . Results obtained at a depth of 25 per cent from the top surface,  $x_3 = 0.75h$

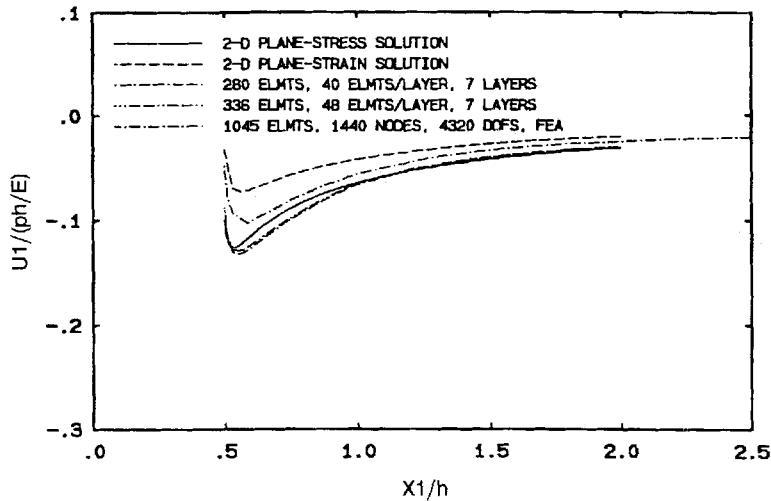


Figure 18. Normalized displacement  $u_1$  versus normalized distance  $x_1$ . Results obtained at a depth of 50 per cent from the top surface,  $x_3 = 0.50h$

shown in Figures 19–21. The numerical results obtained from both the BEM and the FEM are in fairly good agreement. They are situated between the plane-stress and the plane-strain solutions, with the plane-stress solution acting as the lower limit of the three-dimensional solutions.

The BEM results of the displacement  $u_1$  along the  $x_1$  direction show better agreement with the plane-stress solution. Because of the finite thickness of the plate and the fact that the dimensions of the elliptical hole are comparable to the thickness of the plate, the displacements will not be close to the plane-strain solution unless it is observed very close to the surface of the elliptical hole

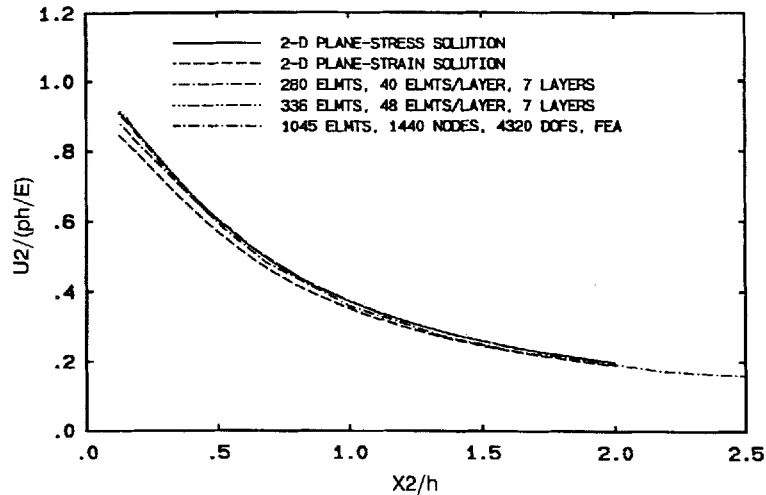


Figure 19. Normalized displacement  $u_2$  versus normalized distance  $x_2$ . Results obtained at a depth of 5 per cent from the top surface,  $x_3 = 0.95h$

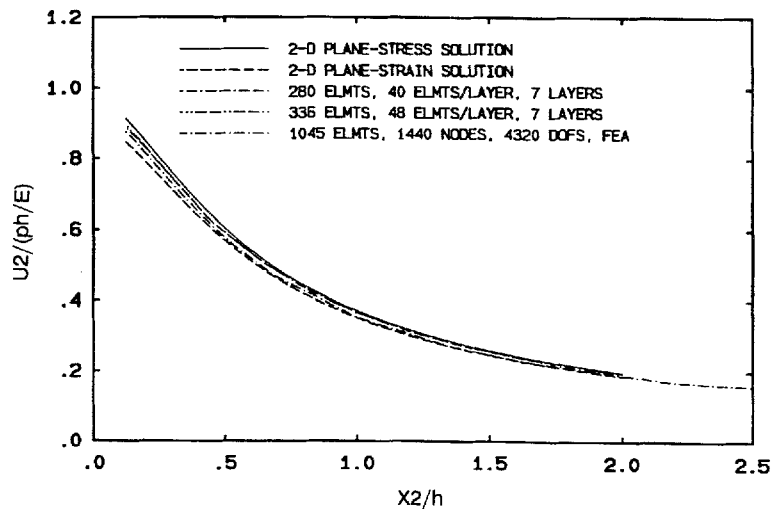


Figure 20. Normalized displacement  $u_2$  versus normalized distance  $x_2$ . Results obtained at a depth of 25 per cent from the top surface,  $x_3 = 0.75h$

and near the midplane of the plate. Figures 22 and 23 show the strain  $\epsilon_{33}$  and the stress ratio  $\sigma_{33}/[\nu(\sigma_{11} + \sigma_{22})]$  respectively, along the  $x_1$  direction obtained by the FEM. Both figures show that the plane-strain conditions cannot be satisfied anywhere along the  $x_1$  direction.

However, Figure 24 shows that  $\sigma_{33}$  approaches zero very quickly at about half the plate thickness away from the surface of the hole, and it remains zero thereafter. Figures 25 and 26 show that the stress components  $\sigma_{11}$  and  $\sigma_{22}$  are independent of  $x_3$  when the distance to the surface of the hole is larger than about three-quarters of the plate thickness. Therefore, the plane-stress conditions are better satisfied and the three-dimensional solution is expected to be closer to the plane-stress solution.

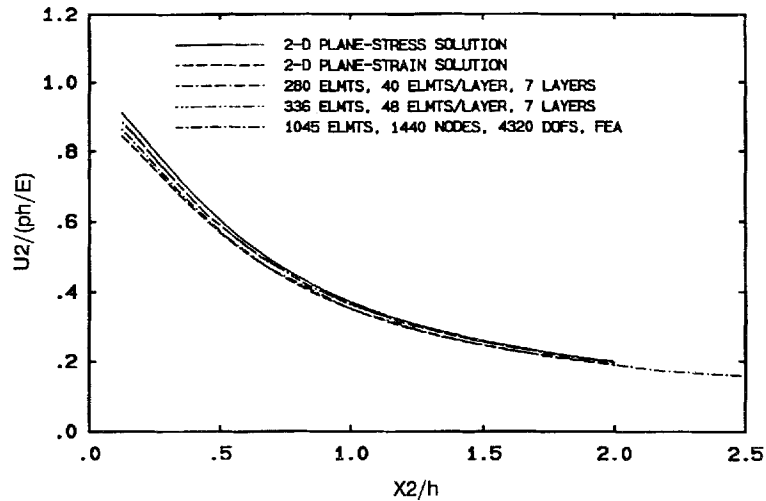


Figure 21. Normalized displacement  $u_2$  versus normalized distance  $x_2$ . Results obtained at a depth of 50 per cent from the top surface,  $x_3 = 0.50h$

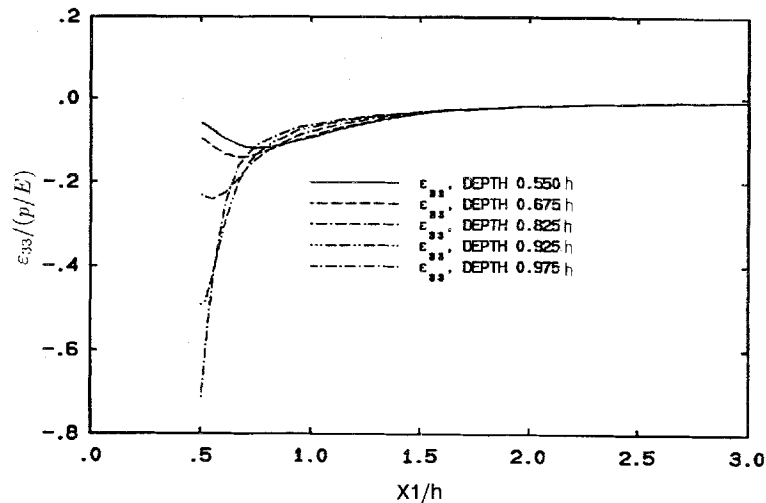


Figure 22. Normalized strain  $\epsilon_{33}$  versus normalized distance  $x_1$ . Results obtained from the FEM analysis

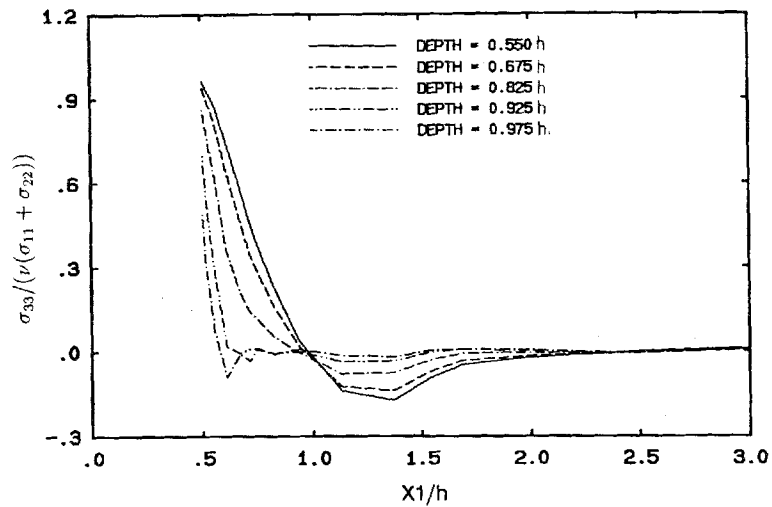


Figure 23. Stress ratio  $\sigma_{33}/(\nu(\sigma_{11} + \sigma_{22}))$  versus normalized distance  $x_1$ . Results obtained from the FEM analysis

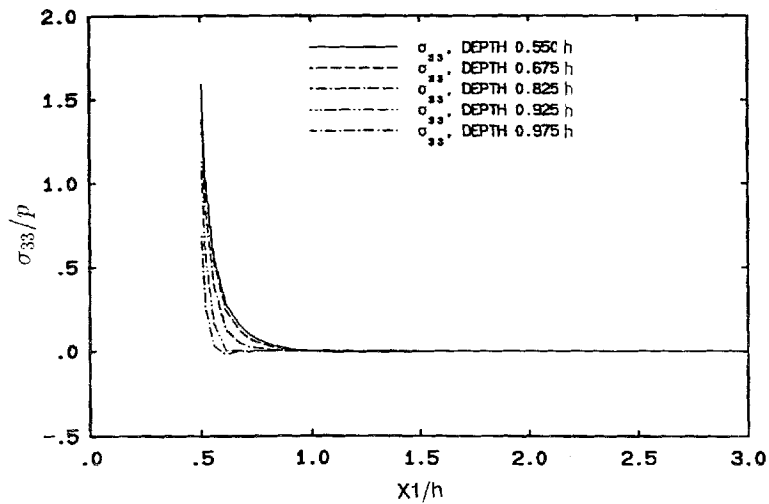


Figure 24. Normalized stress  $\sigma_{33}$  versus normalized distance  $x_1$ . Results obtained from the FEM analysis

Figures 16–18 show that, as the cross section on which the displacement is computed moves towards the midplane of the plate, the displacement  $u_1$  along the  $x_1$  direction obtained from both the BEM and the FEM approaches the plane-stress solution. At the tips of the ellipse, by close observation, the results have a tendency to approach the plane-strain solution.

In the  $x_2$  direction, however, when the displacement  $u_2$  is computed, the BEM and FEM results of the displacement variations of  $u_2$  with respect to  $x_2$  get closer to the plane-strain solutions as the arrays approach the midplane of the plate. This effect is shown in Figures 19–21.

Away from the elliptical hole, the three-dimensional solutions of the displacements  $u_1$  and  $u_2$  are expected to converge to the plane-stress solution. This behaviour is reflected by both the BEM

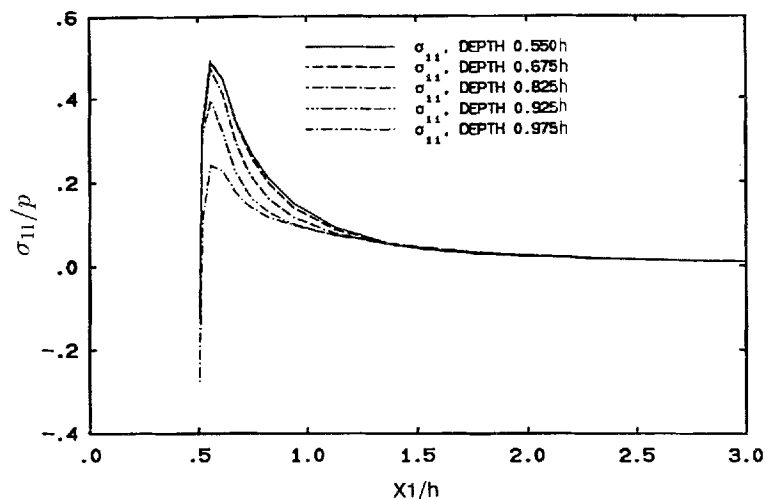


Figure 25. Normalized stress  $\sigma_{11}$  versus normalized distance  $x_1$ . Results obtained from the FEM analysis

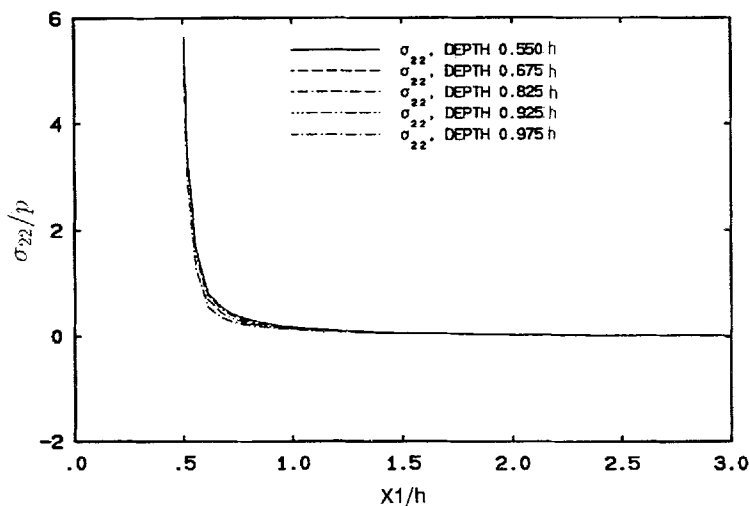


Figure 26. Normalized stress  $\sigma_{22}$  versus normalized distance  $x_1$ . Results obtained from the FEM analysis

and FEM results in Figures 16–26. It also shows clearly that the BEM results of the displacements  $u_1$  and  $u_2$  are in better agreement with the plane-stress solution away from the elliptical hole than the FEM results. The figures also show that the plane-strain solutions get closer and closer to the plane-stress solution as the distance from the surface of the elliptical hole increases. However, the two solutions can never be the same.

*3.4.2. Out-of-plane displacements.* Figures 27–30 show the variations of the normalized displacement  $u_3$  with respect to the normalized distances  $x_1$  and  $x_2$ . The agreement between the

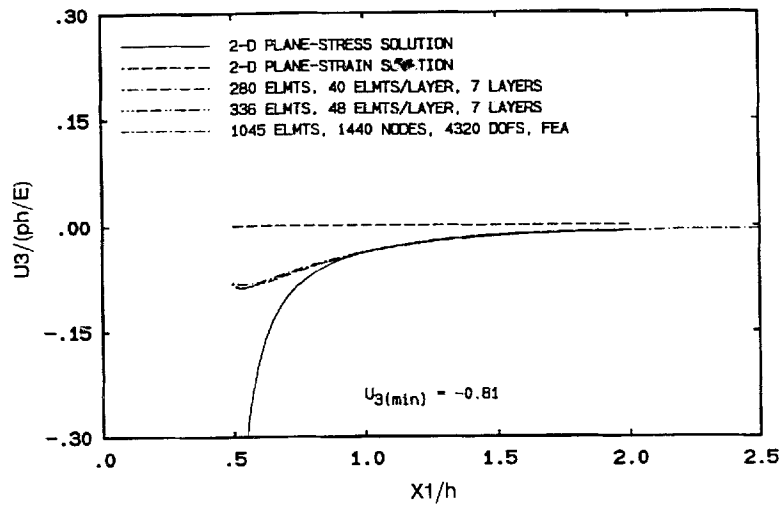


Figure 27. Normalized displacement  $u_3$  versus normalized distance  $x_1$ . Results obtained at a depth of 5 per cent from the top surface,  $x_3 = 0.95h$

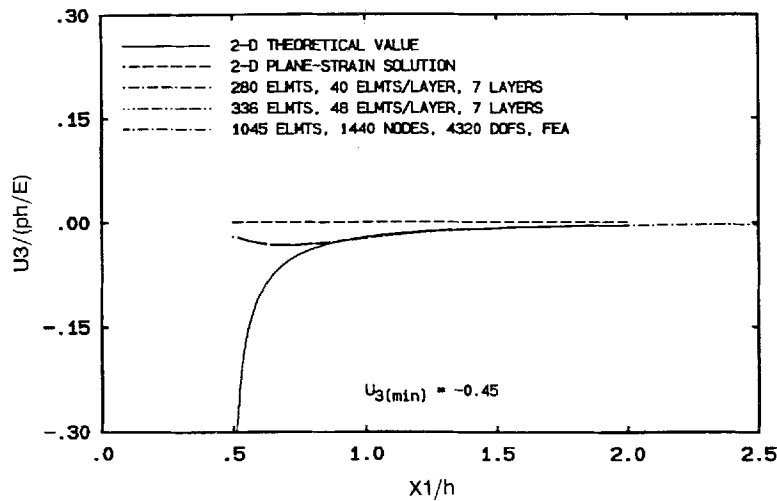


Figure 28. Normalized displacement  $u_3$  versus normalized distance  $x_1$ . Results obtained at a depth of 25 per cent from the top surface,  $x_3 = 0.75h$

proposed BEM and the FEM is excellent. It can be seen from Figures 27 and 28 that the deviation of the three-dimensional numerical results from the two-dimensional plane-stress predictions is dramatic. This deviation is noticeable up to a distance of  $0.5h$  from the tip of the ellipse at the nodal surface, and  $0.4h$  from the tip of the ellipse at the plane three-quarters of the thickness from the lower surface of the plate. This observation is consistent with the analytical, numerical and experimental investigations of the three-dimensional effects near a crack obtained by Yang and

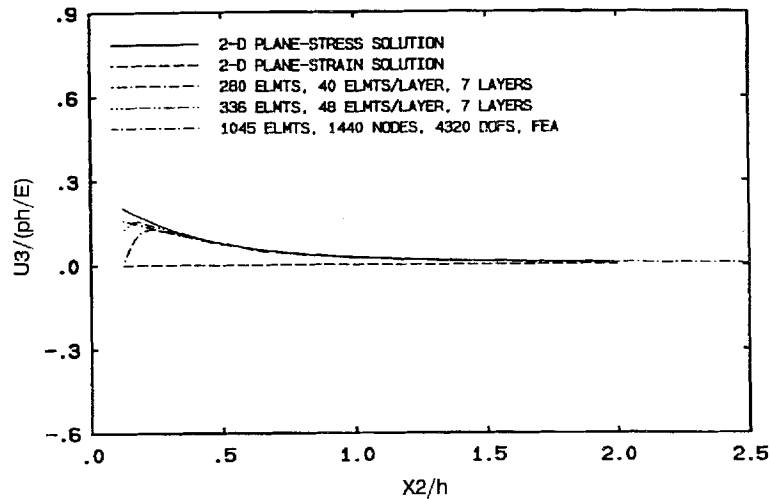


Figure 29. Normalized displacement  $u_3$  versus normalized distance  $x_2$ . Results obtained at a depth of 5 per cent from the top surface,  $x_3 = 0.95h$ .

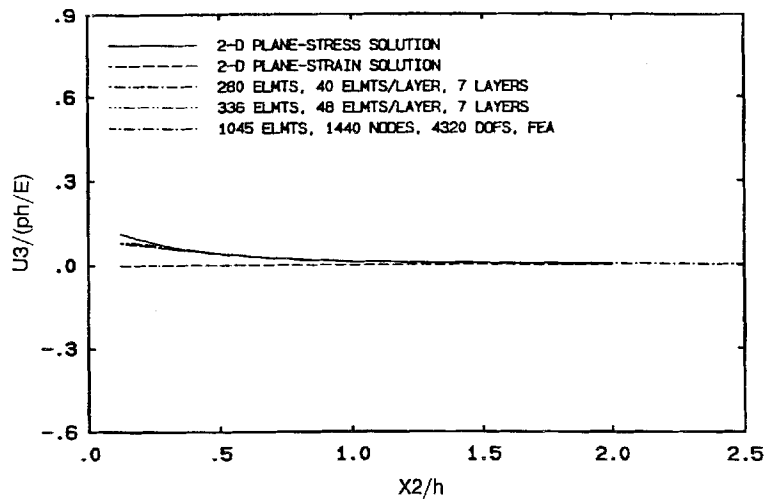


Figure 30. Normalized displacement  $u_3$  versus normalized distance  $x_2$ . Results obtained at a depth of 25 per cent from the top surface,  $x_3 = 0.75h$ .

Freund,<sup>21</sup> Rosakis and Ravi-Chandar<sup>22</sup> and Narasimhan *et al.*<sup>23</sup> As expected,  $u_3$  is identically zero at the midplane.

The plane-stress prediction of  $u_3$  is false near the surface of the hole in the sense that it overpredicts the out-of-plane displacement  $u_3$ . This overprediction of  $u_3$  is caused by the plane-stress assumption  $\sigma_{33} = 0$ . The FEM results in Figure 24 show that  $\sigma_{33}$  does not vanish near the surface of the hole and it presents the feature of stress concentration near the hole.  $\sigma_{33}$  is relatively large ( $\sigma_{33}/(ph/E) = 1.5$ ) near the midplane of the plate as compared to  $\sigma_{33}$  near the

surface of the plate ( $\sigma_{33}/(ph/E) = 0.8$ ).  $\sigma_{33}$  rapidly decreases to almost zero at a distance of half the plate thickness. The physical meaning of the three-dimensional results can be explained as follows. The applied pressure has the tendency to deform the ellipse towards a circle. The tips of the ellipse are stretched by this effect, and thus, the thickness of the plate at the tips of the ellipse decreases. In the plane-stress solution, the stress  $\sigma_{33}$  is zero; therefore, the two-dimensional plane-stress solution will have significantly more out-of-plane displacement,  $u_3$ , than the three-dimensional solution. In addition, near the tips of the ellipse,  $\sigma_{33}$  has a fairly large positive value, which reduces the displacement  $u_3$  more significantly near the surface of the hole than elsewhere. This is the reason that a magnitude decrease in the displacement  $u_3$  is present near the surface of the elliptical hole. This feature does not appear in the pressurized circular problem because of the two-dimensional nature of the problem, in which the actual stress  $\sigma_{33}$  is identically zero.

Figure 29 displays the normalized  $u_3$  versus normalized  $x_2$ , and some discrepancy between the proposed BEM and the FEM is noticeable. This discrepancy is due to the use of large elements on the flatter sides of the ellipse. After local mesh refinement, the result with 336 elements in Figure 29 shows much improvement. It will be shown in a later discussion that in the  $x_2$  direction the thickness variation  $u_3$  also improves very significantly after local mesh refinement. It is expected that the BEM results will converge to the FEM results after further refinement of the meshes for both methods.

The three-dimensional effect in the  $x_2$  direction near the surface of the elliptical hole is confined to within a distance of  $0.3h$  at the nodal plane, and to within a distance of  $0.25h$  at the plane three-quarters of the thickness from the lower surface of the plate.  $u_3$  is identically zero at the midplane of the plate.

*3.4.3. Through-thickness displacements.* The thickness variations of the displacement  $u_1$  along the  $x_1$  direction are shown in Figures 31 and 32. Again, the numerical solutions fall in between the plane-stress and the plane-strain solutions. Two features are worth mentioning. (i) The thickness variations of the numerical results are no longer horizontal straight lines. This feature indicates the three-dimensional nature of the problem. (ii) It can be seen from Figures 31 and 32 that the

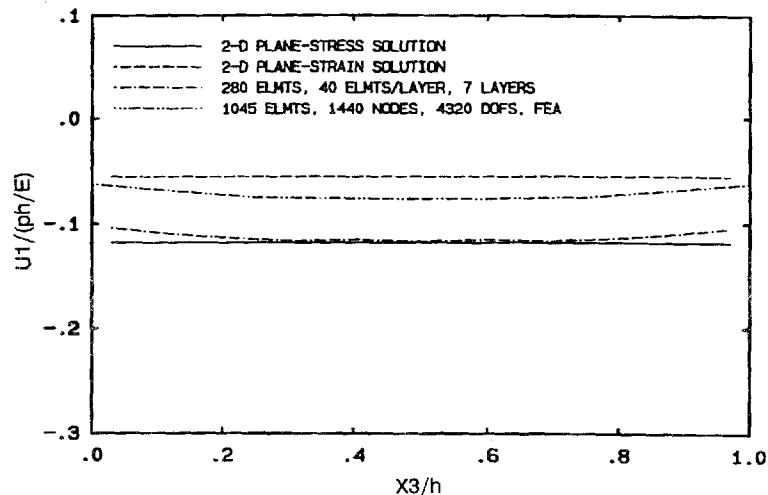


Figure 31. Normalized displacement  $u_1$  versus normalized distance  $x_3$ . Results obtained through the plate thickness at  $x_1 = 0.51h$ ,  $x_2 = 0.00$

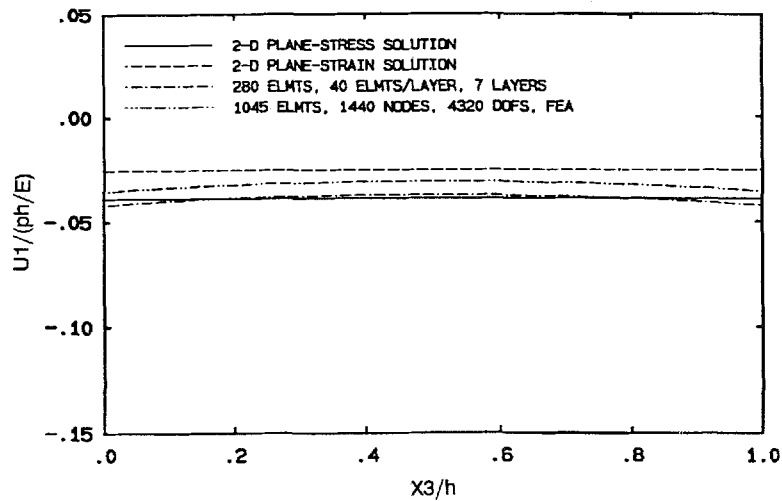


Figure 32. Normalized displacement  $u_1$  versus normalized distance  $x_3$ . Results obtained through the plate thickness at  $x_1 = 1.60h$ ,  $x_2 = 0.00$

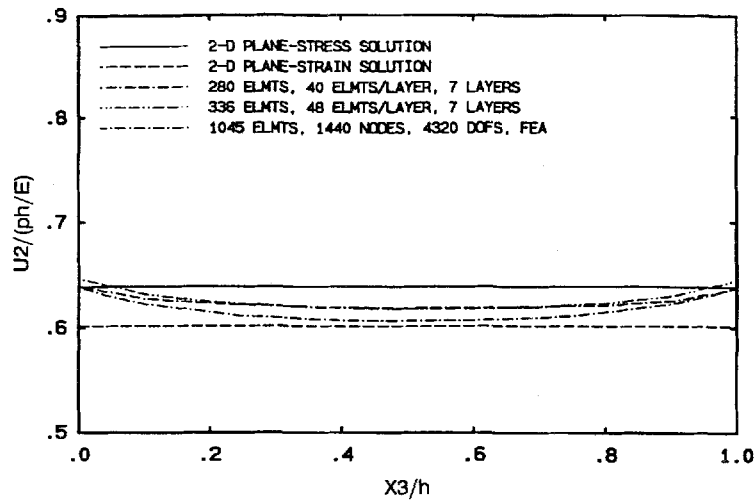


Figure 33. Normalized displacement  $u_2$  versus normalized distance  $x_3$ . Results obtained through the plate thickness at  $x_1 = 0.00$ ,  $x_2 = 0.45h$

numerical solutions approach the plane-stress solutions as the distance to the surface of the hole increases. It can also be seen from these figures that the BEM results converge to the plane-stress solutions better than the FEM results as the distance to the surface of the hole increases. In Figure 32, the scale for the vertical axis is changed in order to explore the detailed features of the thickness variation of  $u_1$  relatively far away from the elliptical hole surface.

Some interesting features are presented in the thickness variations of the displacement  $u_2$  in the direction  $x_3$ . It can be seen from Figure 33 that the displacement  $u_2$  obtained by the proposed BEM using 280 elements deviates from the FEM result. The deviation is most noticeable when

the displacement  $u_2$  is computed near both the surface of the hole and the surface of the plate. After local mesh refinement, the result improves very significantly compared with the FEM results. The two features discussed in the thickness variations of  $u_1$  are also applicable here. The apparent slope discontinuities in the BEM solution are due to the use of relatively large elements along the flatter sides of the ellipse.

Figures 33 and 34 also show that the points near the two surfaces of the plate are displaced more in the  $x_2$  direction than the ones near the midplane of the plate. This phenomenon is due to the constraint difference for points in the plate. There is less constraint on the points near the free surface of the plate than on those near the midplane of the plate. It is easier for a point near the surface of the plate to deform in the  $x_3$  direction than one near the midplane. Because of Poisson's effect, the points near the surfaces of the plate are displaced more in the  $x_2$  direction than those near the midplane of the plate. The above argument can be applied to explain why at the tips of the ellipse the displacement  $u_1$  is less near the free surface than near the midplane.

The most interesting feature lies in the thickness variation of  $u_3$ . As shown here, the out-of-plane displacement is strongly influenced by three-dimensional effects. The thickness variations of  $u_3$  at different distances from the tip of the ellipse along the  $x_1$  direction are shown in Figures 35 and 36. The thickness variations of  $u_3$  along the  $x_2$  direction are shown in Figures 37 and 38. The numerical results of the thickness variations from the proposed BEM agree perfectly with those from the FEM.

Figure 35 shows that, at points close to the tip ( $0.01h$ ),  $u_3$  varies fairly uniformly through the thickness and deviates from zero only when the points are close to the plate surfaces.  $u_3$  varies antisymmetrically with respect to the midplane. The BEM and FEM results are in perfect agreement. Figure 36 shows that the three-dimensional results of the thickness variations of  $u_3$  approach the plane-stress solution, which is linear in  $x_3$  as the distance to the surface of the elliptical hole increases (see (11)). On these plots, the solid line represents the plane-stress solution for  $u_3$ , equation (11), which is linearly dependent on  $x_3$ . It can also be seen that the three-dimensional results fall on top of the plane-stress solution at a distance of about half the plate thickness away from the elliptical hole surface.

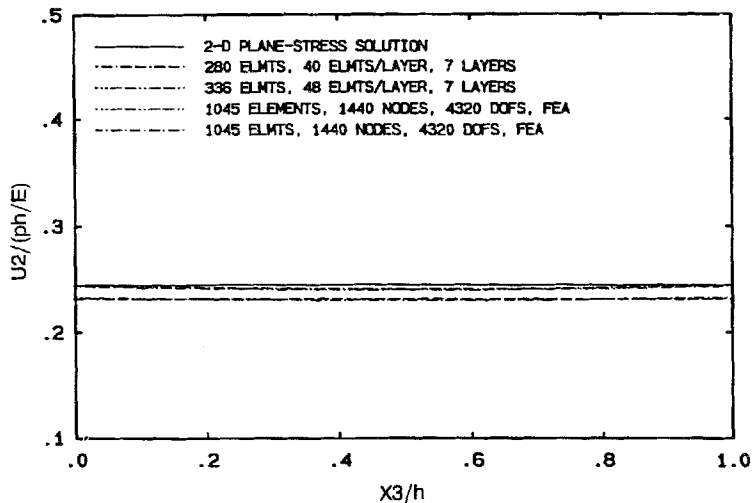


Figure 34. Normalized displacement  $u_2$  versus normalized distance  $x_3$ . Results obtained through the plate thickness at  $x_1 = 0.00$ ,  $x_2 = 1.60h$

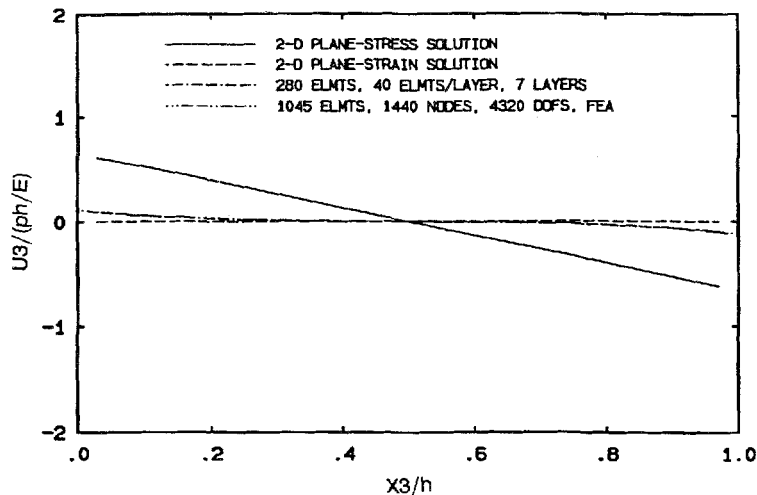


Figure 35. Normalized displacement  $u_3$  versus normalized distance  $x_3$ . Results obtained through the plate thickness at  $x_1 = 0.51h, x_2 = 0.00$

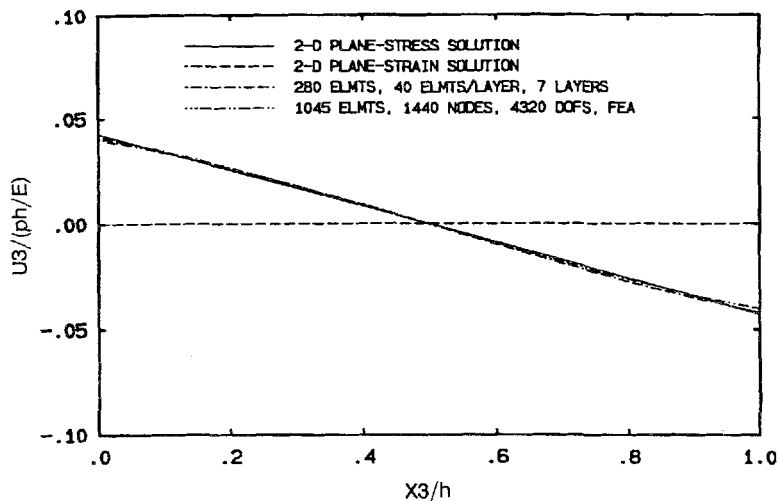


Figure 36. Normalized displacement  $u_3$  versus normalized distance  $x_3$ . Results obtained through the plate thickness at  $x_1 = 1.00h, x_2 = 0.00$

Because of the use of large elements on the flatter sides of the ellipse in the mesh with 280 elements,  $u_3$  in Figure 37 obtained by the proposed BEM shows some deviation from the FEM result when  $u_3$  is computed near the surfaces of the plate. By local mesh refinement and the use of 336 elements in the mesh,  $u_3$  improves very much and is almost the same as the FEM result. There is very little three-dimensional effect present in the  $x_2$  direction. The numerical results quickly converge to the plane-stress solution in this case.

As the distance from the ellipse tip is increased (Figure 38) the three-dimensional numerical variation approaches the plane-stress idealization. Indeed Figure 36 clearly shows that the

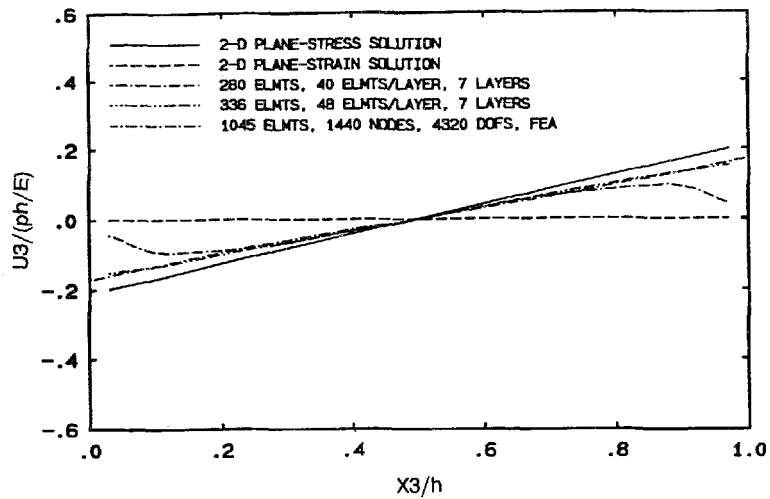


Figure 37. Normalized displacement  $u_3$  versus normalized distance  $x_3$ . Results obtained through the plate thickness at  $x_1 = 0.00$ ,  $x_2 = 0.15h$

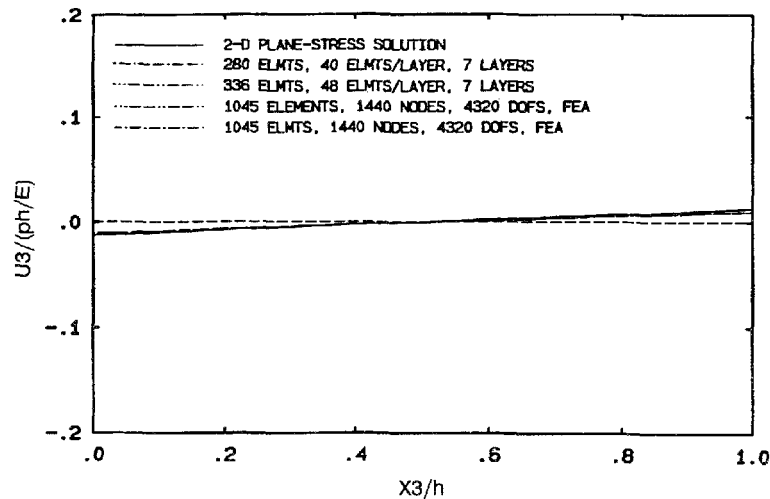


Figure 38. Normalized displacement  $u_3$  versus normalized distance  $x_3$ . Results obtained through the plate thickness at  $x_1 = 0.00$ ,  $x_2 = 1.60h$

three-dimensional solution is well approximated by equation (11) obtained from the plane-stress idealization (linear variation through the thickness). At even greater distances, complete two-dimensional conditions (no variation through the thickness) are achieved.

#### 4. CONCLUSIONS

In this part of the investigation we present numerical examples which demonstrate the applicability of the modified boundary element formulation (see Part I) to the solution of elastostatic

problems involving plate geometries. The accuracy of the procedure is demonstrated by direct comparison with the available analytical solutions. The procedure is also used to quantify the extent of three-dimensional effects at the vicinity of the tips of elliptical holes in plates.

Two pressurized-hole problems have been studied. The results obtained from both the BEM and the FEM are in very good agreement. One very interesting aspect is that the BEM gives better results in  $u_1$  and  $u_2$  when they are obtained relatively far from the surface of the hole as compared to the thickness of the plate. Away from the elliptical hole, the results of both the BEM and the FEM converge to the plane-stress solution, and the results of the BEM agree with the plane-stress solution better than those of the FEM.

It is very important to note that local mesh refinement improves the results considerably. Local mesh refinement on the flatter sides of the ellipse does not have much effect on the results near the tips. This observation makes it possible to use relatively large elements on the flatter sides of the ellipse and refine the elements near the tips without changing the total number of elements.

The study of these problems shows that  $u_1$  and  $u_2$  do not differ from the plane-stress and plane-strain solutions as much as  $u_3$ . The variations of  $u_1$  with respect to  $x_1$  agree better with the plane-stress solution than with the plane-strain solution. In the region near the surface of the hole ( $0.5h \leq x_1 \leq h$ ), the results for  $u_1$  differ from both the plane-stress and the plane-strain solutions due to the three-dimensional effects. However, on the flatter sides of the ellipse, the variations of  $u_2$  with respect to  $x_2$  agree better with the plane-stress solution when they are evaluated near the surfaces of the plate. On the other hand,  $u_2$  thickness variations approach the plane-strain solution when they are computed closer to the midplane of the plate. When the displacements  $u_1$  and  $u_2$  are computed far away from the surface of the elliptical hole, in both problems the BEM results demonstrate better agreement with the plane-stress solution than the FEM results.

The numerical results obtained by the BEM and the FEM show that the  $u_3$  versus  $x_1$  variations for both problems are almost the same except in the region within about  $0.2h$  from the surface of the hole. The sizes of the three-dimensional zones show almost no difference for the two problems. In the  $x_1$ -direction, the three-dimensional zone at a depth of  $0.95h$  is about  $0.5h$ , and the three-dimensional zone size is about  $0.4h$  at a depth of  $0.75h$ . On the other hand, in the  $x_2$ -direction, the sizes of the three-dimensional zones are about  $0.3h$  at a depth of  $0.95h$  and about  $0.25h$  at a depth of  $0.75h$ .

#### ACKNOWLEDGEMENTS

A. J. Rosakis acknowledges the support of the National Science Foundation through the Presidential Young Investigator award MSM8451204. F. G. Benitez is grateful for the support of the Spanish Ministry of Education and Science through grants CICYT PA86-0310 and CICYT MAT91-1014.

#### REFERENCES

1. S. N. Atluri (ed.), 'Computational methods in the mechanics of fracture', in *Computational Methods in Mechanics*, Vol. 2, Elsevier Science Publishers, Amsterdam, 1986.
2. P. D. Hilton and L. N. Gifford, 'Computational fracture mechanics—nonlinear and 3-D problems', *ASME AMD-61*, 1984.
3. A. R. Luxmore and D. R. J. Owen (eds.), *Numerical Methods in Fracture Mechanics*, University College, Swansea, 1978.
4. T. A. Cruse, 'Numerical solutions in three-dimensional elastostatics', *Int. J. Solids Struct.*, **5**, 1259–1274 (1969).
5. T. A. Cruse, 'Lateral constraint in a cracked, three-dimensional elastic body', *Int. J. Fract. Mech.*, **6**, 326–328 (1970).
6. T. A. Cruse, 'Numerical evaluation of elastic stress intensity factors by the boundary-integral equation method', in: J. L. Swedlow (ed.), *The Surface Crack: Physical Problems and Computational Solutions*, ASME, New York, 1972, pp. 153–170.

7. T. A. Cruse, 'Application of the boundary-integral equation method to three-dimensional stress analysis', *J. Comput. Struct.*, **3**, 509-527 (1973).
8. T. A. Cruse, 'An improved boundary integral equation method for three-dimensional elastic stress analysis', *J. Comput. Struct.*, **4**, 741-757 (1974).
9. T. A. Cruse, 'Boundary-integral equation method for three-dimensional elastic fracture mechanics analysis', *AFOSR-TR-75-0813*, 1975.
10. T. A. Cruse and G. J. Meyers, 'Three-dimensional fracture mechanics analysis', *J. Struct. Div. ASCE*, **103**, 309-320 (1977).
11. T. A. Cruse and W. VanBuren, 'Three-dimensional elastic stress analysis of a fracture specimen with an edge crack', *Int. J. Fract. Mech.*, **7**, 1-16 (1971).
12. T. A. Cruse and R. B. Wilson, 'Boundary-integral equation method for elastic fracture mechanics analysis', *AFOSR-TR-78-0355*, 1977.
13. J. Weaver, 'Three-dimensional crack analysis', *Int. J. Solids Struct.*, **13**, 321-330 (1977).
14. G. E. Blandford, A. R. Ingraffea and J. A. Liggett, 'Two-dimensional stress intensity factor computations using the boundary element method', *Int. j. numer. methods eng.*, **17**, 387-404 (1981).
15. M. L. Luchi and A. Poggialini, 'Computation of 3-dimensional stress intensity factors using special boundary elements', in C. A. Brebbia (ed.), *Proc. 5th Int. Conf. on Boundary Element Methods*, Springer, Berlin, 1983, pp. 461-470.
16. F. G. Benitez and A. J. Rosakis, 'Three dimensional elastostatics of a layer and a layered medium', *Division of Engineering and Applied Sciences SM85-21*, California Inst. of Technology, Pasadena, CA, 1985.
17. F. G. Benitez and A. J. Rosakis, 'Three dimensional elastostatics of a layer and a layered medium', *J. Elasticity*, **18**, 3-50 (1987).
18. F. G. Benitez and A. J. Rosakis, 'A modified boundary integral formulation for the study of 3-D crack problems in plates', in *Analytical, Numerical and Experimental Aspects of Three Dimensional Fracture Processes*, ASME AMD-91, 1988, pp. 99-112.
19. L. Lu, 'On the development and application of a modified boundary element method for the analysis of three-dimensional elastostatic problems in thick plates', *Ph.D. Thesis*, California Institute of Technology, Pasadena, CA, 1992.
20. S. P. Timoshenko, J. N. Goodier, *Theory of Elasticity*, 3rd edn, McGraw-Hill, New York, 1970.
21. W. Yang and L. B. Freund, 'Transverse shear effects for through-cracks in an elastic plate', *Int. J. Solids Struct.*, **21**, 977-994 (1985).
22. A. J. Rosakis and K. Ravi-Chandar, 'On crack-tip stress state: an experimental evaluation of three-dimensional effects', *Int. J. Solids Struct.*, **22**, 121-138 (1986).
23. R. Narasimhan, A. J. Rosakis and A. T. Zehnder, 'Three-dimensional fields for a through crack in an elastic-plastic solid: numerical analysis and comparison with interferometry measurements', in *Analytical, Numerical and Experimental Aspects of Three Dimensional Fracture Processes*, ASME AMD-91, 1988, pp. 239-253.
24. O. C. Zienkiewicz, *The Finite Element Method*, McGraw-Hill, London, 1977.